Temperature seasonality in the North American continental interior during the early Eocene climatic optimum

Ethan G. Hyland[1,2*], Katharine W. Huntington[1], Nathan D. Sheldon[3], Tammo Reichgelt[4]

[1] Department of Earth & Space Sciences, University of Washington, Seattle, WA 98195

[2] Department of Marine, Earth & Atmospheric Sciences, North Carolina State University, Raleigh, NC 27695

[3] Department of Earth & Environmental Sciences, University of Michigan, Ann Arbor, MI 48104

[4] Lamont Doherty Earth Observatory, Columbia University, Palisades, NY 10964

Correspondence to: Dr. Ethan G. Hyland (ehyland@ncsu.edu)

Abstract. Paleogene greenhouse climate equability has long been a paradox in paleoclimate research. However, recent developments in proxy and modeling methods have suggested that strong seasonality may be a feature of at least some greenhouse periods. Here we present the first multi-proxy record of seasonal temperatures during the Paleogene from paleofloras, paleosol geochemistry, and carbonate clumped isotope thermometry in the Green River Basin (Wyoming, USA). These combined temperature records allow for the reconstruction of past seasonality in the continental interior, which shows that temperatures were warmer in all seasons during the peak early Eocene climatic optimum and that the mean annual range of temperature was high, similar to the modern value (~26°C). Proxy data and downscaled Eocene regional climate model results suggest amplified seasonality during greenhouse events. Increased seasonality reconstructed for the early Eocene is similar in scope to the higher seasonal range predicted by downscaled climate model ensembles for future high-CO_2 emissions scenarios. Overall, these data and model comparisons have substantial implications for understanding greenhouse climates

in general, and may be important for predicting future seasonal climate regimes and their impacts in continental regions.

1. Introduction

The Paleogene was the last major greenhouse period in Earth's history and is characterized by extreme warming events and resultant biological shifts (e.g., Greenwood and Wing, 1995; Wilf, 2000; Zachos et al., 2001, 2008; McInerney and Wing, 2011), with prolonged warmth during the early Eocene climatic optimum (EECO) peaking from roughly 52 – 50 Ma (e.g. Zachos et al., 2008; Hyland et al., 2017). The early Eocene in general is thought to represent a warm and "equable" global climate state with high mean annual temperatures (MAT; e.g., Wilf, 2000; Zachos et al., 2008), low mean annual range of temperatures (MART; e.g., Wolfe, 1978, 1995; Greenwood and Wing, 1995), and low pole-to-equator temperature gradients (LTG; e.g., Spicer and Parrish, 1990; Greenwood and Wing, 1995; Evans et al., 2018). While high MAT during the Eocene now seems well established, the feasibility of "equable" conditions defined by low MART and low LTG is still in question as a result of increasingly complex global climate models which are unable to reproduce such conditions (e.g., Barron, 1987; Sloan and Barron, 1990; Sloan, 1994; Huber and Caballero, 2011; Lunt et al., 2012).

Recent proxy work on Paleogene warm intervals and hyperthermals such as the Paleocene-Eocene thermal maximum (PETM) has suggested that continental interiors may maintain higher or near-modern MART during these periods, implying that the "low seasonality" aspect of climate equability may not be reasonable under all greenhouse conditions (e.g., Snell et al., 2013; Eldrett et al., 2014). Despite this suggestion, it remains unclear whether proxy estimates from other basins, regions, and greenhouse periods can be reconciled with the range of feasible conditions provided by climate model studies. Quantitative reconstructions of

seasonality (MART) based on precise proxy estimates of mean annual temperature (MAT), warm month mean temperature (WMMT), and cold month mean temperature (CMMT) could help to resolve some of these model-proxy discrepancies by providing a robust and well-constrained set of seasonal observations for comparison to available climate model outputs. Robust proxy reconstructions of seasonality are crucial for understanding this aspect of past greenhouse equability (Lunt et al., 2012; Snell et al., 2013; Peppe, 2013).

Seasonality estimates have previously been made using a variety of proxy paleothermometers in isolation, and can now be made with higher confidence using recently developed methods that target each of these individual temperature parameters: MAT can be estimated using a paleosol geochemistry-based thermometer, WMMT can be estimated using the carbonate clumped isotope (Δ_{47}) thermometer, and CMMT can be estimated using a nearest living relative (NLR) floral coexistence thermometer. The bulk major-element geochemistry of modern soils has been used to quantify the effects of weathering processes via a wide range of geochemical indices (see Sheldon and Tabor, 2009). The relationship between modern climate parameters like temperature and indices such as salinization (Sheldon et al., 2002), the paleosol weathering index (Gallagher and Sheldon, 2013), and the paleosol-paleoclimate model (Stinchcomb et al., 2016) has led to the development of climofunctions for MAT that have been used to estimate paleo-MAT during the Cenozoic (e.g., Retallack, 2007; Takeuchi et al., 2007; Bader et al., 2015; Stinchcomb et al., 2016). The clumped isotope (Δ_{47}) thermometer is based on the temperature-dependent relative enrichment of multiply substituted isotopologues of $CaCO_3$ ($^{13}C^{18}O^{16}O_2$) within the solid carbonate phase, which is independent of the isotopic composition of the water in which the carbonate precipitated (e.g., Ghosh et al., 2006; Eiler, 2007). For pedogenic carbonates in temperate regions, this growth temperature is linked to mean warm

season soil temperatures (e.g., Quade et al., 2013; Hough et al., 2014), and has been used to estimate paleo-WMMT during the Cenozoic (e.g., Snell et al., 2013; Garzione et al., 2014). The nearest living relative (NLR) coexistence method has been developed based on the sensitive and highly conserved collective modern cold temperature tolerances of related floras to calculate cold month temperatures (e.g., Wolfe, 1995; Mosbrugger and Utescher, 1997). Those relationships have been refined and used to estimate quantitative paleo-CMMT during the Cenozoic (e.g., Greenwood et al., 2005; Thompson et al., 2012; Eldrett et al., 2014; Utescher et al., 2014; Greenwood et al., 2017).

Here we employ a multi-proxy approach using paleosol geochemistry, clumped isotope, and floral NLR coexistence thermometry methods from the same localities in order to address seasonality in the past, specifically applying it to the issue of early Eocene greenhouse equability in the North American continental interior. We estimate MAT, WMMT, and CMMT throughout the EECO including both defined peak (~51 Ma) and non-peak conditions (e.g., Hyland et al., 2017), and compare the resultant proxy estimates of temperature seasonality (MART) to the modern climate state of the region, as well as to downscaled climate model predictions of temperature seasonality during the Eocene and for future emissions scenarios.

2. Methods

The targeted early Eocene locality is the Green River Basin (GRB) in southwestern Wyoming (USA; Figure 1). The GRB sequence is composed of a series of terrestrial clastic rocks deposited during the early Eocene and EECO as a result of Laramide synorogenic fluvial and lacustrine sedimentation along the margin of endorheic paleo-lake Gosiute (e.g., Clyde et al., 2001; Smith et al., 2008, 2010, 2015). Contemporaneous multi-proxy records of peak and non-

peak conditions during the EECO are from the interfingering Wasatch Formation, primarily fluvial sandstones and paleosols of the Ramsey Ranch and Cathedral Bluffs Members, and Green River Formation, primarily lacustrine shales and carbonates of the Wilkins Peak Member (Figure 1). The paleosols and pedogenic carbonates were sampled from the Honeycomb Buttes near South Pass, Wyoming (42.24°N, 108.53°W; Hyland and Sheldon, 2013), while the floral assemblages were sampled from the Latham coal (41.68°N, 107.88°W), Sourdough coal (41.91°N, 108.00°W), Niland Tongue (41.06°N, 108.77°W), and Little Mountain quarry (41.28°N, 109.30°W) outside Rock Springs, Wyoming (Figure 1; Wilf, 1998; 2000).

2.1 Temperature proxies

2.1.1 Paleosol geochemistry

The bulk major-element geochemistry of modern soils (specifically B horizons) has been used extensively to develop a number of composition-climate relationships, including those predicted by the paleosol-paleoclimate model ($PPM_{1.0}$), which relates a broad suite of major element compositions to mean annual temperature (among other factors) at the site of soil formation (Stinchcomb et al., 2016). Stinchcomb et al. (2016) developed this nonlinear spline model using the largest available geochemical dataset from 685 modern soils across North America in order to derive proxy relationships between 11 major and minor oxides and MAT. This new proxy is calibrated over a wider range of climatic conditions, soil types, and parent materials than other available proxies (c.f., Sheldon et al., 2002; Gallagher and Sheldon, 2013), and has been validated via independent comparisons in both modern climosequences (Stinchcomb et al., 2016) and Miocene paleosols (Driese et al., 2016). Following associated

procedures, our bulk paleosol samples from selected upper Bt horizons of defined Alfisols (described in detail by Hyland and Sheldon, 2013) were prepared for major-element geochemistry by cleaning and grinding to a homogenous powder. Samples were analyzed using lithium borate fusion preparation and X-ray fluorescence (XRF) measurements at ALS Chemex Laboratory (Vancouver, BC), where analytical uncertainty for analyses was maintained at less than 0.1% for all elements, and replicate analyses had a mean standard deviation of 0.8% (*Table A.1*). Resultant major and minor element data were not corrected for loss-on-ignition (e.g., Stinchcomb et al., 2016), and were input into the open-access $PPM_{1.0}$ model, which produces "low", "best" and "high" MAT estimates; we present the "high" estimates as MAT here (see *Section 4.1* for explanation; *Table A.1*). Broadly, soil geochemical proxies are consistent with other paleoclimate proxies (e.g., paleobotanical; Sheldon and Tabor, 2009 and references therein), and are more robust to diagenetic alteration under a wide variety of burial conditions (Hyland and Sheldon, 2016).

2.1.2 Clumped isotope geochemistry

The clumped isotope (Δ_{47}) thermometer is based on the theoretical temperature dependence of the overabundance of multiply substituted carbonate ion isotopologues (primarily $^{13}C^{18}O^{16}O_2^{-2}$) within the solid carbonate phase, which is independent of the isotopic composition of the waters from which the carbonate precipitated (e.g., Schauble et al., 2006; Ghosh et al., 2006; Eiler, 2007). The enrichment of "clumped" isotopologues relative to the abundance expected for a random distribution of isotopes among isotopologues (Δ_{47}) varies with the growth temperature of the sampled carbonate (e.g., Ghosh et al., 2006; Dennis et al., 2011; Zaarur et al., 2013; Kluge et al., 2015; Kelson et al., 2017). Clumped isotope thermometry of soil carbonates is

a useful paleoenvironmental proxy in continental settings (e.g., Eiler, 2011; Quade et al., 2013), and studies of recent pedogenic carbonates indicate that their clumped isotope values record environmental temperature conditions during mineral growth. The timing of pedogenic carbonate growth is controlled by a combination of soil moisture, CO_2, temperature, and other factors over 10^2–10^4 years (e.g., Cerling, 1984; Cerling and Quade, 1993; Breecker et al., 2009; Zamanian et al., 2016), and clumped isotope analyses show corresponding variability in recorded temperatures (e.g., Peters et al., 2013; Hough et al., 2014; Burgener et al., 2016; Ringham et al., 2016; Gallagher and Sheldon, 2016). However, for pedogenic carbonates forming in forest soils from mid-latitude regions, this growth temperature has been shown to be linked to mean warm season soil temperatures in most settings (e.g., Breecker et al., 2009; Passey et al., 2010; Quade et al., 2013; Garzione et al., 2014; Hough et al., 2014; Ringham et al., 2016), and has been used to estimate paleo-WMMT during the Cenozoic (e.g., Suarez et al., 2011; Snell et al., 2013; Quade et al., 2013; Garzione et al., 2014).

Pedogenic carbonate nodules from selected Bk horizons (paleosol depths ~20–240 cm) were thin-sectioned and analyzed under transmitted light and cathodoluminescence to identify primary micritic carbonate (Figure 2), which was microdrilled/homogenized for clumped isotope (Δ_{47}) analysis. Extremely shallow (<50 cm) or deep (>200 cm) carbonates were analyzed specifically to examine temperature depth profiles in paleosols (Figure 2), while pedogenic carbonates from commonly sampled depths (50–200 cm; e.g., Cerling, 1984; Koch, 1998; Zamanian et al., 2016) were used for calculating and interpreting paleotemperature records. Powdered samples and carbonate standards were analyzed in replicate at the University of Washington's IsoLab, following methods of Burgener et al. (2016) and Kelson et al. (2017), which are modified after Huntington et al. (2009) and Passey et al. (2010). Briefly, CO_2 is

produced from 6–8 mg of pure carbonate reacted in a common phosphoric acid bath (~105% H_3PO_4) at 90°C. Evolved CO_2 is then cleaned via passage through a series of automated cryogenic traps and a cooled (-20°C) Poropak Q column using helium carrier gas through a nickel and stainless steel vacuum line, and the purified CO_2 is transferred to Pyrex break seals. Each sample is then analyzed on a Thermo MAT253 mass spectrometer equipped with an automated 10-port tube cracker inlet system and configured to measure m/z 44–49, using data acquisition methods and scripts presented by Schauer et al. (2016).

All analyses include an automatically-measured pressure baseline (PBL; He et al., 2012), are corrected using heated gas (1000°C; Huntington et al., 2009) and CO_2-water equilibration (4°C, 60°C) lines during the corresponding analysis period (*Table B.1*), and are reported in the absolute reference frame (ARF; Dennis et al., 2011). Following recent work (Daëron et al., 2016; Schauer et al., 2016), mass spectrometer data are corrected using the ^{17}O correction values recommended by Brand et al. (2010). Carbonate standards for these analyses include international standards NBS-19 and ETH-2, as well as internal standards C64 and COR, which are all reported relative to VPDB ($\delta^{13}C$, $\delta^{18}O$) and ARF (Δ_{47}) in *Table B.1*. All samples were analyzed in replicate (3–5) to minimize standard analytical error, and data were reduced following Schauer et al. (2016). Carbonate growth temperatures ($T[\Delta_{47}]$) were calculated using the most current and extensive inorganic calcite calibration (Kelson et al., 2017), which was produced using the updated ^{17}O correction values of Brand et al. (2010) and is consistent with our analytical methods. Based on preliminary comparisons, the Kelson et al. (2017) calibration produces results not significantly different from data calculated using previous calibrations at moderate Earth-surface temperatures (~20–40°C; Daëron et al., 2016; C. John and M. Daëron, pers. comm., 2016; *Table B.1*).

185

186 **2.1.3 Floral coexistence analysis**

187 Floral physiognomy and floral coexistence techniques are often applied in concert to
188 arrive at terrestrial paleoclimate estimates (e.g. Spicer et al., 2014; Reichgelt et al., 2015; West et
189 al., 2015). While floral leaf physiognomy has been used to develop character-climate
190 relationships for parameters like CMMT and MART (e.g., Wolfe, 1995; Wolfe et al., 1998;
191 Wing, 1998), other work has raised questions about the reliability of modern calibrations and
192 possible covariability of seasonal temperatures recorded by floral methods (Jordan, 1997; Peppe
193 et al., 2010). Similar questions have been raised regarding the nearest living relative (NLR)
194 coexistence method (Grimm and Denk, 2012; Grimm and Potts, 2016). However, recent
195 developments have addressed these issues including: 1) improvements or revisions to NLR
196 assignments for paleofloral assemblages (e.g., Manchester et al., 2014; SIMNHP, 2015), 2) new
197 global datasets of modern floral distributions (e.g., TROPICOS, 2015; USDA, 2015, GBIF,
198 2016), 3) high-resolution linked climatic datasets (e.g., Hijmans et al., 2005), and 4) the
199 application of more rigorous statistical analyses (e.g., Eldrett et al., 2014; Utescher et al., 2014;
200 Harbert and Nixon, 2015). As a result of this work, bioclimatic analysis has emerged as a refined
201 version of this approach, employing the climatic range of modern living relatives of plants found
202 together in a fossil assemblage and statistically constraining the most likely climatic co-
203 occurrence envelope (e.g., Greenwood et al., 2005; Thompson et al., 2012; Eldrett et al., 2014;
204 Greenwood et al., 2017).

205 Fossil assemblages were selected from the literature (e.g., Wilf, 1998, 2000) based on
206 temporal fit, floristic diversity, and reliable taxonomy. Fossil taxa were each attributed to a
207 modern taxon based on nearest living relative (e.g., MacGinitie, 1969; Hickey, 1977; Manchester

208 and Dilcher, 1982; Wolfe and Wehr, 1987; Wing, 1998; Wilf, 1998, 2000; Manchester et al.,
209 2014; SIMNHP, 2015), with unattributed or disputed placements assigned conservatively at
210 higher taxonomic levels (*Table C.1*). Climatic envelopes of modern groups in North America
211 and Asia were retained for the ancient taxa based on environmental niche conservation (e.g.,
212 Wang et al., 2010; Fang et al., 2011). Modern taxa distributions (GBIF, 2016) were linked to
213 high-resolution gridded climatic maps (Hijmans et al., 2005) to extract MAT, WMMT and
214 CMMT using the Dismo Package in the R Statistical Program (R Core Team, 2013). Prior to
215 calculating climatic ranges, plant distribution coordinate files were scrutinized for: 1) plants with
216 dubious taxonomic assignments, as not all identifications were rigorous and not all collected
217 specimens were taxonomically assigned by experts (only species-level identifications are
218 included); 2) plants occurring outside of their natural ranges, as many plants occur outside their
219 adapted environment due to agricultural or aesthetic translocation; and 3) redundant occurrences,
220 as many duplicate coordinates or researcher entries exist for the same taxon and their inclusion
221 may skew results toward given localities.
222 Quantitative paleotemperatures were estimated using a modified bioclimatic analysis
223 approach (e.g., Greenwood et al., 2005; Thompson et al., 2012; Eldrett et al., 2014; Greenwood
224 et al., 2017). Overlap ranges of climatic tolerances for coexisting species from each assemblage
225 were defined by calculating probability density functions of those climatic envelopes (Figure 3
226 and *Table C.2*) consistent with recent work (e.g., Thompson et al., 2012; Harbert and Nixon,
227 2015; Grimm and Potts, 2016; Greenwood et al., 2017). In order to avoid inclusion of apparent
228 coexistence intervals in which no modern occurrence is recorded, we calculate the collective
229 probability density of taxa co-occurrence for each combination of MAT (x), WMMT (y), and
230 CMMT (z):

$$f(x|t) = \frac{1}{\sqrt{2\sigma^2\pi}} e^{-\frac{(x-\mu)^2}{2\sigma^2}} \quad (1)$$

$$f(y|t) = \frac{1}{\sqrt{2\sigma^2\pi}} e^{-\frac{(y-\mu)^2}{2\sigma^2}} \quad (2)$$

$$f(z|t) = \frac{1}{\sqrt{2\sigma^2\pi}} e^{-\frac{(z-\mu)^2}{2\sigma^2}} \quad (3)$$

$$f(x,y,z,t) = \ln\left[\left(f(x) \times f(y) \times f(z)\right)_{t1} \times \ldots \times \left(f(x) \times f(y) \times f(z)\right)_{tn}\right] \quad (4)$$

Calculations are repeated such that the likelihood (*f*) is calculated for each climatic combination, for each taxon (*t*), dependent on the number of taxa (*n*), using the mean and standard deviation of each taxon (*Table C.2*). Climate input parameters were individual occurrence data points (~32,000) derived from GBIF (2016), excluding combinations unlikely to represent the climatic envelope of the taxa in the assemblage by calculating a maximum likelihood probability density function that defines a precise estimate of temperature parameters with a low standard deviation for each selected assemblage (Figure 3).

2.2 Modern climate data and model downscaling

The modern temperature dataset was derived from 1981–2010 averaged climate normals from National Oceanic and Atmospheric Administration (NOAA) weather observation stations within the Green River Basin (n = 18; NCDC, 2010), defined as the area 40.5–43°N by 107–110.5°W (Figure 1). Future model temperature projection results used a 10-model ensemble from the Coupled Model Intercomparison Project Phase 5 (CMIP5) under standard low (RCP4.5) and high (RCP8.5) emissions scenarios (IPCC, 2014); specifics of each model/configuration are available from the World Climate Research Programme (2011). Results were averaged monthly for the final 10 years of the model run (2090–2099) and calculated over the same study area

using standard bias-correction and spatial downscaling (BCSD) methods developed by PCDMI (2014). Eocene model temperature results used data from a modified three-dimensional regional climate model (RegCM3; Sewall and Sloan, 2006; Pal et al., 2007) with established Eocene boundary conditions including low (560 ppm; LoCO) and high (2240 ppm; HiCO) atmospheric pCO_2 scenarios (Sewall and Sloan, 2006; Thrasher and Sloan, 2009; 2010); specifics of the model configurations can be found in Thrasher and Sloan (2009). Those results were averaged for the final 20 years of the model run at equilibrium and calculated over the same study area (40.5–43°N by 107–110.5°W) by integrating data across grid cells monthly for each model year within the above defined Green River Basin (e.g., Snell et al., 2013). This particular set of Eocene model configurations was chosen because it allows for the highest available resolution over the basin domain using the best available set of boundary conditions (c.f., EoMIP; Lunt et al., 2012). All modern climate normals and model downscaling results are reported in *Table D.1*.

3. Results

$PPM_{1.0}$ statistical model results for MAT from these paleosol samples range from 13.5 to 17.6°C (μ = 15.2°C; σ = 1.3°C). Uncertainty for these estimates is reported as the root mean squared error of the model fit regression (±2.5°C). Petrographic observation of carbonate nodules from all depths and selected soils identified dominantly micritic textures with minor components of sub-angular quartz grains and occasional sparry (>20μm) calcite veins and cements; however, we were able to identify and micro-sample unaltered fine-grained (<5μm) calcite material in each of the examined samples (n = 14; Figure 2). Clumped isotope Δ_{47} values for these samples range from 0.582 to 0.631‰ (μ = 0.607‰; σ = 0.014‰), which corresponds to an estimated WMMT range of 18 to 34°C (μ = 25°C; σ = 4°C). Uncertainty for these estimates is reported as

propagated error from analytical and equilibrated CO_2 reference frame uncertainty (negligible); replicate standard error (μ = 0.008‰) or standard error from long-term standards, whichever is larger; and calibration standard error (e.g., Kelson et al., 2017); which have a combined error averaging ±3°C. Clumped isotope-based temperature depth profiles in the sampled paleosols show no clear trend with depth, and estimates are mostly within error for a given paleosol (Figure 2). Nearest living relative bioclimatic analysis minimum cold tolerances for these samples range from -28 to 24°C (μ = 6°C; σ = 7°C), and maximum warm tolerances range from 10 to 43°C (μ = 28°C; σ = 5°C). Probability density functions define bioclimatic envelopes (Figure 3) corresponding to an estimated CMMT range of 4.2 to 7.6°C (μ = 5.9°C; σ = 1.2°C), an MAT range of 15.2 to 18.2°C (μ = 16.5°C; σ = 1.1°C), and a WMMT range of 27.9 to 28.7°C (μ = 28.3°C; σ = 0.3°C) for the collective floral assemblages. Uncertainty for these estimates is reported as 2σ for individual assemblage PDF distributions, which average ±2°C. Proxy estimates from all three methods show a trend of increasing temperatures from non-peak conditions into the peak EECO (~51 Ma), after which temperatures decreased back to lower values (Figure 4).

Modern climate normals averaged monthly for the GRB range from -8.4 to 18.1°C, with a MAT of 4.4°C (*Table D.1*). Downscaled Eocene climate model results averaged monthly for the GRB range from 4 to 24°C (LoCO) and 6 to 30°C (HiCO), with MATs of 13°C and 16°C, respectively (*Table D.1*). Downscaled future climate model results averaged monthly for the GRB range from -5.0 to 20.4°C (RCP4.5) and -2.9 to 24.7°C (RCP8.5), with MATs of 7.1°C and 10.6°C, respectively (*Table D.1*). Monthly temperature trends maintain roughly the same shape for modern observational data, future model estimates, and Eocene model estimates. However, the Eocene modeled cases show substantially higher winter temperatures, and in both modern

298 and Eocene modeled cases the higher emission/pCO_2 scenario shows an enhanced summer signal
299 relative to the lower emission/pCO_2 scenario from the same time period (Figure 5).
300
301 **4. Discussion**
302
303 **4.1 Temperature estimates**
304 Temperature estimates from the $PPM_{1.0}$ spline model are based on specifically selected
305 uppermost B horizons of paleosols with comparable parent materials. These horizons were
306 selected based on previous work describing and sampling paleosols from the Cathedral Bluffs
307 Member in the GRB (Figure 1; Hyland and Sheldon, 2013), and based on the characteristics of
308 soils sampled for the paleosol paleoclimate model dataset (Stinchcomb et al., 2016), in order to
309 generate the most robust input data for the $PPM_{1.0}$ spline model. While the $PPM_{1.0}$ model
310 produces multiple possible estimates of paleo-MAT, the estimate shown to be most reliable via
311 concurrent comparisons with other paleotemperature methods (paleobotanical and paleosol
312 proxies) is the "high MAT" value we present here (Michel et al., 2014; Stinchcomb et al., 2016;
313 Driese et al., 2016). We further justify our use of the "high" estimate because the $PPM_{1.0}$ training
314 dataset heavily samples soils from temperate regions (specifically the conterminous USA) which
315 tend to have lower MAT (≤10°C) and therefore could place excess weight on low values in the
316 model predictive space. This sampling bias likely produces the demonstrated pattern of "best"
317 MAT predictions generally exhibiting positive residuals (Stinchcomb et al., 2016), which means
318 that the $PPM_{1.0}$ model would be more likely to skew temperature estimates from paleosol and
319 other modern samples toward lower-than-observed MAT values. The presented mean annual
320 temperatures appear to coincide with a statistical mean between CMMT and WMMT estimates

(Figure 4), and also agree within uncertainty with independent MAT estimates from other types of paleosol geochemistry (salinization index, $\delta^{18}O$; Hyland and Sheldon, 2013) and broadly with updated physiognometric (*Table C.3*; Wilf, 2000) and coexistence analysis paleobotanical estimates from the GRB (Figure 4).

Based on the assessment of physical and isotopic data, our sampled pedogenic carbonate nodules appear to be primary records of Earth surface temperatures at the time of their formation. All sampled nodules preserve micritic carbonate, and transmitted light and cathodoluminescence images show limited recrystallization or void-filling spar and no evidence of pervasive remineralization (Figure 2). Clumped isotopic data also suggest primary and uncontaminated carbonate material; Δ_{48} values remain low (<<1‰; *Table B.1*), indicating a lack of hydrocarbon or sulfide contamination (e.g., Guo and Eiler, 2007; Huntington et al. 2009). Temperature and $\delta^{18}O$ measurements remain well within the range of reasonable terrestrial values, particularly for continental interior basins with seasonal climates (*Table B.1*; e.g., Quade et al., 2013; Hough et al., 2014). Carbonates forming in temperate regions often exhibit summer/warm-month temperatures due to warm, dry conditions and low soil CO_2 concentrations during those months (e.g., Breecker et al., 2009; Quade et al., 2013). Such conditions are predicted for the GRB during the early Eocene based on regional climate models (Thrasher and Sloan, 2009; 2010), and are evident in paleosol features (Clyde et al., 2001; Hyland and Sheldon, 2013) as well as evaporative $\delta^{18}O$ of source waters from nearby paleo-lakes Gosiute and Uinta (*Table B.1*; e.g., Sarg et al., 2013; Frantz et al., 2014). Further warm biasing of soil temperature with respect to air temperature can be imparted by radiant ground heating, but such effects are likely negligible in shaded forest soils (e.g., Quade et al., 2013; Ringham et al., 2016). Clumped isotope data from two soil depth profiles collected in the GRB agree within uncertainty below ~50 cm (Figure 2),

suggesting that surface heating and depth attenuation of surface temperature variability does not significantly affect the samples used for our MART reconstructions (paleosol depths ~50–200 cm; e.g., Ringham et al., 2016).

These results imply that the temperatures measured from our pedogenic carbonates broadly reflect warm month mean soil temperatures (WMMT) as observed in other records (e.g., Peters et al., 2013; Hough et al., 2014; Burgener et al., 2016). Possible exceptions are two samples at the base of the Honeycomb Buttes section (HB-109 and HB-18; *Table B.1*) which appear to correspond to MAT estimates from the same paleosols ($PPM_{1.0}$; Figure 4). These lowest temperature estimates from the base of the section may be artificially "cool" as a function of seasonal precipitation regimes spreading carbonate formation across other parts of the year, particularly in soils with deeper Bk horizons like these (e.g., Gallagher and Sheldon, 2016). Because of the likely bias toward MAT in these two samples, we exclude them from calculations of WMMT or MART as indicated in Figure 4; additionally, this effect means that all of our clumped isotope-based estimates of WMMT may be artificially low, suggesting that our calculated MART values could represent a minimum value. However, our resultant clumped isotope-based temperature estimates are mostly in agreement with both regional climate model predictions of summer month air temperatures (e.g., Thrasher and Sloan, 2009; Snell et al., 2013) and paleobotanical coexistence estimates of warm month mean temperatures (Figure 4).

Paleobotanical coexistence methods have been shown to reconstruct paleo-temperatures robustly, particularly for warm and cold months in well-sampled and taxonomically rich localities such as these (e.g., Thompson et al., 2012; Grimm and Potts, 2016). However, uncertainties may be larger than accounted for by the described statistical methods applied to these assemblages because: 1) many fossil classifications within the GRB assemblages are not

directly comparable to or identifiable as extant species, and coexistence analyses at a generic or familial level may introduce bias by broadening the temperature tolerance ranges of most groups (e.g., Wang et al., 2010); and 2) evolutionary or climatic preferences of Paleogene fossil taxa may not be fully conserved in extant groups, introducing potential sources of error (e.g., Fang et al., 2011). If we double estimated error to account for these unquantifiable uncertainties, the collective coexistence probability density functions from these assemblages still produce CMMT, MAT, and WMMT estimates defined by narrow "maximum likelihood" bioclimatic envelopes (< ±3°C; Figure 3; *Table C.2*), which suggest that the environmental characteristics of these fossil assemblages are well constrained despite some higher-level NLR assignments. Additionally, sampling bias from well-sampled temperate regions (e.g., North America) in the modern GBIF database may place undue weight on the cool end of plant ranges (e.g., Greenwood et al., 2017), constraining paleotemperature estimates to lower values or smaller ranges than is appropriate. This suggests that, similar to clumped isotope-based estimates, our plant-based MART values could also represent a minimum value. Despite this, paleobotanical coexistence CMMT estimates agree with regional climate model predictions of winter month temperatures in the GRB (e.g., Thrasher and Sloan, 2009; 2010), MAT estimates agree broadly with multiple paleosol-based proxy estimates (Figure 4; Hyland and Sheldon, 2013) and with updated paleobotanical physiognomy estimates (Figure 4; *Table C.3*; Wilf, 2000), and WMMT estimates agree with regional climate model estimates (e.g., Thrasher and Sloan, 2009; Snell et al., 2013) and broadly with clumped isotope-based estimates (Figure 4). Taken together these proxy results paint a consistent picture of Earth-surface temperatures during the early Eocene, despite uncertainties inherent in each individual method.

390 **4.2 Temperature seasonality**

391 Because each of these proxies appears to represent different seasonal temperatures
392 robustly, we combine these estimates to produce a new multiply constrained investigation of
393 paleo-MART. By calculating the differences between CMMT from paleobotanical coexistence
394 analysis, MAT from paleosol geochemistry or paleobotanical analyses, and WMMT from Δ_{47}
395 composition or paleobotanical coexistence analysis, we can directly estimate MART in the past
396 and compare differences in seasonal temperatures independent of calculation method (c.f., Snell
397 et al., 2013). In other words, our approach can define MART as: 1) the difference between
398 WMMT and CMMT; or 2) twice the difference between MAT and either WMMT or CMMT,
399 assuming that MAT falls half way between those estimates by definition (Table 1). Because our
400 approach can calculate MART using both methods and an average of multiple proxies, this
401 allows for a wide range of independent checks on our estimates, providing the most robust
402 available paleo-MART (Table 1). Each method provides consistent answers that are statistically
403 indistinguishable for a given time period (Student's *t*-test p-values = 0.4–0.9), lending
404 confidence to calculations which show that MART ranged from 21–26°C during the early
405 Eocene (Table 1).

406 By averaging all data from each population (CMMT, MAT, WMMT) for the peak and
407 non-peak intervals separately, calculated MARTs suggest that seasonality was generally slightly
408 lower than modern across parts of the early Eocene (~21–23°C, non-peak), but appears to have
409 increased to near-modern ranges during the peak EECO (~26°C; Figure 4; Table 1). The
410 calculated uncertainty of the difference between these populations (S.E.D) is ~4°C, which makes
411 the non-peak and peak intervals statistically distinct though nearly overlapping. Overall, this

412 suggests that not only is seasonality not reduced during greenhouse periods (e.g., Snell et al.,
413 2013), it may actually be expanded (Figure 5).

414 Estimates from the lower end of our reconstructed MART range are still higher than
415 MART estimates from individual paleobotanical proxies (15–18°C; e.g., Greenwood and Wing,
416 1995; Wolfe et al., 1998), but compare favorably to estimates from regional climate models with
417 assumed lacustrine or paludal land cover (20–22°C; Thrasher and Sloan, 2010). However,
418 estimates from the higher end of the reconstructed MART range compare more favorably to
419 modeled MART values with assumed woodland or forested land cover (24–26°C; Thrasher and
420 Sloan, 2010; Snell et al., 2013). The transient nature of paleo-lake Gosiute and the variable
421 evolution of environments within the GRB throughout the early Eocene is well documented in
422 stratigraphic archives, indicating that the basin may have been alternately dominated by the
423 paleo-lake or by forested floodplains during this period (Smith et al., 2008; 2014). In this
424 context, our results suggest that both lower (though still in excess of any previous paleobotanical
425 estimates) and higher MART states may in fact be reasonable for this region at different points
426 during the early Eocene as the GRB evolved. Moreover, proxy and modeling work does not
427 appear to be contradictory, instead having captured different portions of the range of possible
428 MART values indicated for the peak vs. non-peak EECO in this part of the continental interior
429 (Figures 4 and 5). Regardless, these results suggest that MART values lower than ~20°C (e.g.,
430 Greenwood and Wing, 1995; Wolfe et al., 1998) may be unreasonable during any part of the
431 EECO, even in the context of variable climate and environmental conditions. This is particularly
432 true because MART estimates using these proxy methods are more likely to underestimate than
433 overestimate seasonality (see Section 4.1).
434

4.3 Seasonality implications

Our new proxy data and model comparisons have important implications for continental climates, as they suggest two potential characteristics of seasonality in interior regions during warming events: 1) proxies tend to indicate continental temperatures on the high end of modeled ranges in all seasons, and 2) both proxies and regional models indicate that summer temperatures may increase disproportionately, actually broadening MART, at high atmospheric pCO_2. While proxy and model estimates of paleotemperature generally agree through the early Eocene in the GRB, proxy estimates consistently fall in the top half of all modeled values (Figure 5). Although these model and proxy results are not statistically distinct, they may suggest that realistic environmental responses could have a skewed distribution within the range of model-predicted climate outcomes, an observation which has been made previously for other regions and time periods (e.g., Roe and Baker, 2007; Diffenbaugh and Field, 2013).

Winter temperatures were generally high during the Eocene (Figures 4 and 5; e.g., Greenwood and Wing, 1995), but during the peak EECO summer temperatures appear to have increased disproportionally, broadening the range of MART (Figures 4 and 5). While this apparent trend may be related to the lack of direct CMMT estimates during the peak EECO, the consistency of MART estimates using both reconstruction methods (see Section 4.2) suggests the observation is robust. Regional Eocene climate model output for the GRB predicts lower MART (~20°C) under low pCO_2 conditions (LoCO scenario), and higher MART (~24°C) under high pCO_2 conditions (HiCO scenario; Figure 5; *Table D.1*). Therefore, a theoretical transition from lower (≤500 ppm) to higher (≥1000 ppm) atmospheric pCO_2 during the peak EECO (e.g., Hyland and Sheldon, 2013; Jagniecki et al., 2015) could effectively broaden MART and result in extreme summer temperatures during that period, which would be consistent with both regional

458 model and proxy predictions in the GRB (Figure 5). Regional model-proxy agreement on the
459 plausibility of variable moderate to high MART (20–26°C) in continental interiors fits with
460 global simulations employing a reasonable set of radiative forcings and climate sensitivities,
461 which project similar seasonality ranges during this and other greenhouse events (Huber and
462 Caballero, 2011; Lunt et al., 2012). These temperature seasonality estimates also corroborate
463 recent work on other regions and warm periods (e.g., Snell et al., 2013; Eldrett et al., 2014), and
464 further support the interpretation that continental interiors were less "equable" than previously
465 thought under greenhouse conditions (Snell et al., 2013; Peppe, 2013).

466 Increased seasonality and the disproportionate response of summer temperatures during
467 greenhouse climates also has significant implications for predicting future change in continental
468 interiors. Current projections for the next century using downscaled global climate model
469 ensembles (PCDMI, 2014; *Table D.1*) indicate generally increased temperatures and changing
470 seasonality in North America, and GRB temperatures are projected to increase particularly
471 during winter months (Figure 5). However for high emissions scenarios that may be closer in
472 character to greenhouse conditions like the peak EECO or the PETM (RCP8.5; e.g., IPCC, 2007;
473 Lunt et al., 2012), summer temperatures in the GRB increase more strongly, broadening MART
474 (Figure 5; *Table D.1*). This trend in MART from peak EECO proxy data and high-
475 emission/pCO_2 model simulations in both the future and Eocene suggests a potential atmospheric
476 pCO_2 threshold for enhanced seasonality, and provides support for models and observations
477 indicating that continental interiors may experience more extreme seasonality in the future under
478 heightened greenhouse conditions (e.g., IPCC, 2007; Diffenbaugh and Field, 2013; Diffenbaugh
479 et al., 2017). The mechanism for producing this increased seasonality remains unclear and
480 requires further study in terms of both proxy applications and model development, although

changes in land cover may play a crucial role at least in regional variability (Thrasher and Sloan, 2010; Diffenbaugh and Field, 2013).

5. Conclusions

Estimates of winter (paleofloral NLR coexistence), mean (paleosol geochemistry), and summer (clumped isotope) temperatures from the early Eocene in the Green River Basin of Wyoming (USA) provide new multi-proxy constraints on seasonality (mean annual range of temperature) in terrestrial settings during greenhouse periods. These records show that MART was variable but near (or above) modern values during the early Eocene climatic optimum, confirming both that seasonality in continental interiors may not remain constant, and that EECO conditions likely do not conform to at least the seasonality aspect of greenhouse "equability". Comparisons between proxy data and regional/downscaled climate models further imply that temperature seasonality may respond differently at low vs. high atmospheric pCO_2. Overall, this suggests that our understanding of past greenhouse climates in continental interiors may be incomplete when it comes to "equability", and proposes the potential for extreme seasonality in these regions during past warming events and in the future, which likely has important implications for natural ecosystems and human infrastructure.

Data Availability. Summarized paleosol, isotope, floral, and modeling data are available in the Supplement, and detailed sample or locality data are available from the authors on request.

Author Contributions. EGH, NDS, and KWH designed the study; EGH and NDS collected the samples and conducted fieldwork; EGH conducted laboratory analyses; EGH, KWH, and TR conducted data analyses and reduction; all authors contributed to the writing of the manuscript.

Competing Interests. The authors declare that they have no conflicts of interest.

Acknowledgments. The authors thank D. Peppe, K. Snell, and XXX for manuscript comments; A. Schauer, L. Burgener, and P. Wilf for assistance with proxy data; PCDMI, WCRP, L. Sloan, and J. Sewall for archived modeling datasets; NSF grants EAR-1252064 and 1156134 (KWH), GSA's Farouk El-Baz grant (EGH), and the Quaternary Research Center and Future of Ice Initiative at the University of Washington for funding and support.

References.

Bader, N.E., Nicolaysen, K.P., Maldonado, R.L., Murray, K.E., and Mudd, A.C.: Extensive middle Miocene weathering interpreted from a well-preserved paleosol, Cricket Flat, Oregon, USA, Geoderma, 239, 195–205, 2015.

Barron, E.: Eocene equator-to-pole surface ocean temperatures: A significant climate problem?, Paleoceanography, 2, 729–739, 1987

Brand, W.A., Assonov, S.S., and Coplen, T.B.: Correction for the ^{17}O interference in $\delta^{13}C$ measurements when analyzing CO_2 with stable isotope mass spectrometry, Pure Appl. Chem., 82, 1719–1733, 2010.

Breecker, D.O., Sharp, Z.D., and McFadden, L.D.: Seasonal bias in the formation and stable isotopic composition of pedogenic carbonate in modern soils from central New Mexico, USA, Geol. Soc. Am. Bull., 121, 630–640, 2009.

Burgener, L., Huntington, K., Hoke, G., Schauer, A., Ringham, M., Latorre, C., and Diaz, F.: Variations in soil carbonate formation and seasonal bias over >4km of relief in the western Andes (30°S) revealed by clumped isotope thermometry, Earth Planet. Sc. Lett., 441, 188–199, 2016.

Cerling, T.E.: The stable isotopic composition of modern soil carbonate and its relationship to climate, Earth Planet. Sci. Lett., 71, 229–240, 1984.

Cerling, T.E., and Quade, J.: Stable carbon and oxygen isotopes in soil carbonates, Geophys. Mono., 78, 217–231, 1993.

Clyde, W.C., Sheldon, N.D., Koch, P.L., Gunnell, G.F., and Bartels, W.S.: Linking the Wasatchian/Bridgerian boundary to the Cenozoic Global Climate Optimum: new magnetostratigraphic and isotopic results from South Pass, Wyoming, Palaeogeogr. Palaeocl., 167, 175–199, 2001.

Daëron, M., Blamart, D., Peral, M., and Affek, H.: Absolute isotopic abundance ratios and the accuracy of Δ_{47} measurements, Chem. Geol., 442, 83–96, 2016.

Dennis, K.J., Affek, H.P., Passey, B.H., Schrag, D.P., and Eiler, J.M.: Defining and absolute reference frame for clumped isotope studies of CO_2, Geochim. Cosmochim. Ac., 75, 7117–7131, 2011.

Diffenbaugh, N.S., and Field, C.B.: Changes in ecologically critical terrestrial climate conditions, Science, 341, 486–492, 2013.

Diffenbaugh, N.S., Singh, D., Mankin, J.S., Horton, D.E., Swain, D.L., Touma, D., Charland, A., Liu, Y., Haugen, M., Tsiang, M., and Rajaratnam, B.: Quantifying the influence of global warming on unprecedented extreme climate events, P. Natl. Acad. Sci. USA, 114, 4881–4886, 2017.

548 Driese, S.G., Peppe, D.J., Beverly, E.J., DiPietro, L.M., Arellano, L.N., and Lehmann, T.:
549 Paleosols and paleoenvironments of the early Miocene deposits near Karunga, Lake Victoria,
550 Kenya, Palaeogeogr. Palaeocl., 443, 167–182, 2016.

551 Eiler, J.M.: Clumped-isotope geochemistry – The study of naturally-occurring, multiply-
552 substituted isotopologues, Earth Planet. Sc. Lett., 262, 309–327, 2007.

553 Eiler, J.M.: Paleoclimate reconstruction using carbonate clumped isotope thermometry: Quat.
554 Sci. Rev., 30, 3575–3588, 2011.

555 Eldrett, J.S., Greenwood, D.R., Polling, M., Brinkhuis, H., and Sluijs, A.: A seasonality trigger
556 for carbon injection at the Paleocene-Eocene Thermal Maximum, Clim. Past, 10, 759–769, 2014.

557 Evans, D., Sagoo, N., Renema, W., Cotton, L.J., Muller, W., Todd, J.A., Saraswati, P.K.,
558 Stassen, P., Ziegler, M., Pearson, P.N., Valdes, P.J., and Affek, H.P.: Eocene greenhouse climate
559 revealed by coupled clumped isotope-Mg/Ca thermometry, P. Natl. Acad. Sci. USA, 115, 1174–
560 1179, 2018.

561 Fang, J., Wang, Z., and Tang, Z.: Atlas of woody plants in China: Distribution and climate,
562 Springer-Verlag (Beijing, CH), 1909 pp., 2011.

563 Frantz, C.M., Petryshyn, V.A., Marenco, P.J., Tripatic, A., Berelson, W.M., and Corsetti, F.A.:
564 Dramatic local environmental change during the Early Eocene Climatic Optimum detected using
565 high-resolution chemical analyses of Green River stromatolites, Palaeogeogr. Palaeocl., 405, 1-
566 15, 2014.

567 Gallagher, T.M., and Sheldon, N.D.: A new paleothermometer for forest paleosols and its
568 implications for Cenozoic climate, Geology, 41, 647–650, 2013.

569 Gallagher, T.M., and Sheldon, N.D.: Combining soil water balance and clumped isotopes to
570 understand the nature and timing of pedogenic carbonate formation, Chem. Geol., 435, 79–91,
571 2016.

572 Garzione, C.A., Auerbach, D.J., Smith, J.J., Rosario, J.J., Passey, B.H., Jordan, T.E., and Eiler,
573 J.M.: Clumped isotope evidence for diachronous surface cooling of the Altiplano and pulsed
574 surface uplift of the Central Andes, Earth Planet. Sci. Lett., 393, 173–181, 2014.

575 Ghosh, P., Adkins, J., Affek, H., Balta, B., Guo, W., Schauble, E., Schrag, D., and Eiler, J.: ^{13}C-
576 ^{18}O bonds in carbonate minerals: a new kind of paleothermometer, Geochim. Cosmochim. Ac.,
577 70, 1439–1456, 2006.

578 Global Biodiversity Information Facility (GBIF): Open Access Biodiversity Data: http://gbif.org
579 (last accessed July 2016).

580 Greenwood, D.R., and Wing, S.L.: Eocene continental climates and latitudinal temperature
581 gradients, Geology, 23, 1044–1048, 1995.

582 Greenwood, D.R., Archibald, S.B., Mathewes, R.W., and Moss, P.T.: Fossil biotas from the
583 Okanagan Highlands, southern British Columbia and northeastern Washington State: Climates
584 and ecosystems across an Eocene landscape, Can. J. Earth Sci., 42, 167–185, 2005.

585 Greenwood, D.R., Keefe, R.L., Reichgelt, T., and Webb, J.A.: Eocene paleobotanical altimetry
586 of Victoria's Eastern Uplands, Aus. J. Earth Sci., 64, 625–637, 2017.

587 Grimm, G.W., and Denk, T.: Reliability and resolution of the coexistence approach- A
588 revalidation using modern day data, Rev. Palaeobot. Palyno., 172, 33–47, 2012.

589 Grimm, G.W., and Potts, A.: Fallacies and fantasies: the theoretical underpinnings of the
590 coexistence approach for paleoclimate reconstructions, Clim. Past, 12, 611–622, 2016.

591 Guo, W., and Eiler, J.M.: Temperatures of aqueous alteration and evidence for methane
592 generation on the parent bodies of the CM chondrites, Geochim. Cosmochim. Ac., 71, 5565–
593 5575, 2007.

594 Harbert, R., and Nixon, K.: Climate reconstruction analysis using coexistence likelihood
595 estimation (CRACLE): A method for the estimation of climate using vegetation, Am. J. Bot.,
596 102, 1277–1289, 2015.

597 He, B., Olack, G., and Colman, A.: Pressure baseline correction and high-precision CO_2 clumped
598 isotope (Δ_{47}) analysis by gas-source isotope ratio mass spectrometry, J. Mass Spectrom., 44,
599 1318–1329, 2012.

600 Hickey, L.: Stratigraphy and paleobotany of the Golden Valley Formation (early Tertiary) of
601 western North Dakota, Geol. Soc. Am. Mem., 150, 183 pp., 1977.

602 Hijmans, R.J., Cameron, S.E., Parra, J.L., Jones, P.G., and Jarvis, A.: Very high resolution
603 interpolated climate surfaces for global land areas, Intl. J. Climatol., 25, 1965–1978, 2005.

604 Hough, B.G., Fan, M., and Passey, B.H.: Calibration of the clumped isotope geothermometer in
605 soil carbonate in Wyoming and Nebraska, USA: Implications for paleoelevation and
606 paleoclimate reconstruction, Earth Planet. Sc. Lett., 391, 110–120, 2014.

607 Huber, M., and Caballero, R.: The early Eocene equable climate problem revisited, Clim. Past, 7,
608 603–633, 2011.

609 Huntington, K.W., Eiler, J.M., Affek, H.P., Guo, W., Bonifacie, M., Yeung, L.Y., Thiagarajan,
610 N., Passey, B., Tripati, A., Daeron, M., and Came, R.: Methods and limitations of clumped CO_2
611 isotope (Δ_{47}) analysis by gas-source isotope ratio mass spectrometry, J. Mass Spectrom., 44,
612 1318–1329, 2009.

613 Hyland, E.G., and Sheldon, N.D.: Coupled CO_2-climate response during the Early Eocene
614 Climatic Optimum, Palaeogeogr. Palaeoclim., 369, 125–135, 2013.

615 Hyland, E.G., and Sheldon, N.D.: Examining the spatial consistency of palaeosol proxies:
616 Implications for palaeoclimatic and palaeoenvironmental reconstructions in terrestrial
617 sedimentary basins, Sedimentology, 63, 959–971, 2016.

618 Hyland, E.G., Sheldon, N.D., and Cotton, J.M.: Constraining the early Eocene climatic optimum:
619 A terrestrial interhemispheric comparison: Geol. Soc. Am. Bull., 129, 244–252, 2017.

Intergovernmental Panel on Climate Change (IPCC): Fourth Assessment Report: Climate Change (AR4), In Pachuari, R.K., and Reisinger, A. (Eds.), IPCC (Geneva, SWI), 104 pp., 2007.

Intergovernmental Panel on Climate Change (IPCC): Fifth Assessment Report: Climate Change (AR5), In Pachuari, R.K., and Meyer, L.A. (Eds.), IPCC (Geneva, SWI), 151 pp., 2014.

Jagniecki, E.A., Lowenstein, T.K., Jenkins, D.M., and Demicco, R.V.: Eocene atmospheric CO_2 from the nahcolite proxy, Geology, 43, 1075–1078, 2015.

Jordan, G.J.: Uncertainty in paleoclimatic reconstructions based on leaf physiognomy, Aus. J. Bot., 45, 527–547, 1997.

Kelson, J., Huntington, K.W., Schauer, A., Saenger, C., and Lechler, A.: Toward a universal carbonate clumped isotope calibration: Diverse synthesis and preparatory methods suggest a single temperature relationship, Geochim. Cosmochim. Ac., 197, 104–131, 2017.

Kluge, T., John, C., Jourdan, A., Davis, S., and Crawshaw, J.: Laboratory calibration of the calcium carbonate clumped isotope thermometer in the 25 - 250°C temperature range, Geochim. Cosmochim. Ac., 157, 213–227, 2015.

Koch, P.L.: Isotopic reconstruction of past continental environments, Annu. Rev. Earth Plant. Sci., 26, 573–623, 1998.

Lunt, D., Jones, T., Heinemann, M., Huber, M., LeGrande, A., Winguth, A., Loptson, C., Marotzke, J., Roberts, C., Tindall, J., Valdes, P., and Winguth, C.: A model-data comparison for a multi-model ensemble of early Eocene atmosphere-ocean simulations: EoMIP, Clim. Past, 8, 1717–1736, 2012.

MacGinitie, H.D.: The Eocene Green River Flora of northwestern Colorado and northeastern Utah, University of California Press (Berkeley, CA), 201 pp., 1969.

Manchester, S., and Dilcher, D.: Pterocaryoid fruits in the Paleogene of North America and their evolutionary and biogeographic significance, Am. J. Bot., 69, 275–286, 1982.

Manchester, S.R.: Revisions to Roland Brown's North American Paleocene flora, Ac. Mus. Natl. Prag., 70, 153–210, 2014.

McInerney, F.A., and Wing, S.L.: The Paleocene-Eocene Thermal Maximum: A perturbation of carbon cycle, climate and biosphere with implications for the future, Ann. Rev. Earth Planet. Sci., 39, 489–516, 2011.

Michel, L.A., Peppe, D.J., Lutz, J.A., Driese, S.G., Dunsworth, H.M., Harcourt-Smith, W., Horner, W.H., Lehmann, T., Nightingale, S., and McNulty, K.P.: Remnants of an ancient forest provide ecological context for Early Miocene fossil apes, Nat. Commun., 5, 3236, 2014.

Mosbrugger, V., and Utescher, T.: The coexistence approach- a method for quantitative reconstructions of tertiary terrestrial palaeoclimate data using plant fossils, Palaeogeogr. Palaeocl., 134, 61–86, 1997.

National Climatic Data Center (NCDC): United States Climate Normals, 1981–2010: Climatography of the US, National Oceanic and Atmospheric Administration, http://www.ncdc.noaa.gov/data#normals (last accessed April 2015).

Pal, J.S., et al. (19 others): The ICTP RegCM3 and RegCNET: Regional climate modeling for the developing world, Bull. Am. Meteorol. Soc., 88, 1395–1409, 2007.

Passey, B.H., Levin, N., Cerling, T.E., Brown, F., and Eiler, J.: High-temperature environments of human evolution in East Africa based on bond ordering in paleosol carbonates, P. Natl. Acad. Sci. USA, 107, 11245–11249, 2010.

Peppe, D.J., Royer, D.L., Wilf, P., and Kowalski, E.: Quantification of large uncertainties in fossil leaf paleoaltimetry, Tectonics, 29, TC3015, 2010.

Peppe, D.J.: Hot summers in continental interiors: The case against equability during the early Paleogene, Geology, 41, 95–96, 2013.

Peters, N., Huntington, K.W., and Hoke, G.: Hot or not? Impact of seasonally variable soil carbonate formation on paleotemperature and O-isotope records from clumped isotope thermometry, Earth Planet. Sc. Lett., 361, 208–218, 2013.

Program for Climate Model Diagnosis and Intercomparison (PCDMI): Bias corrected and downscaled World Climate Research Programme's Coupled Model Intercomparison Project phase 5 (CMIP5) climate projections, http://gdo-dcp.ucllnl.org/downscaled_cmip_projections/, 2014.

Quade, J., Eiler, J., Daeron, M., and Achyuthan, H.: The clumped isotope geothermometer in soil and paleosol carbonate, Geochim. Cosmochim. Ac., 105, 92–100, 2013.

R Core Team: R: A language and environment for statistical computing: Foundation for Statistical Computing (Vienna, AT), https:/www.r-project.org, 2013.

Reichgelt, T., Kennedy, E.M., Conran, J.G., Mildenhall, D.C., and Lee, D.E.: The early Miocene paleolake Manuherikia: vegetation heterogeneity and warm-temperate to subtropical climate in southern New Zealand, J. Paleolimnol., 53, 349–365, 2015.

Retallack, G.J.: Cenozoic paleoclimate on land in North America, J. Geol., 115, 271-294, 2007.

Ringham, M.C., Hoke, G.D., Huntington, K.W., and Aranibar, J.N.: Influence of vegetation type and site-to-site variability on soil carbonate clumped isotope records, Andean piedmont of Central Argentina (32–34 °S), Earth Planet. Sc. Lett., 440, 1–11, 2016.

Roe, G.H., and Baker, M.B.: Why is climate sensitivity so unpredictable?, Science, 318, 629–632, 2007.

Sarg, J.F., Suriamin, H., Tanavsuu-Milkeviciene, K., and Humphrey, J.D.: Lithofacies, stable isotopic composition, and stratigraphic evolution of microbial and associated carbonates, Green River Formation (Eocene), Am. Assc. Petr. Geol. Bull, 97, 1937–1966, 2013.

690 Schauble, E.A., Ghosh, P., and Eiler, J.M.: Preferential formation of ^{13}C-^{18}O bonds in carbonate
691 materials estimated using first-principle lattice dynamics, Geochim. Cosmochim. Ac., 70, 2510–
692 2529, 2006.

693 Schauer, A.J., Kelson, J., Saenger, C., and Huntington, K.W.: Choice of ^{17}O correction affects
694 clumped isotope (Δ_{47}) values of CO_2 measured with mass spectrometry, R. Comm. Mass
695 Spectrom., 30, 2607–2616, 2016.

696 Sewall, J., and Sloan, L.: Come a little bit closer: A high-resolution climate study of the early
697 Paleogene Laramide foreland, Geology, 34, 81–84, 2006.

698 Sheldon, N.D., and Tabor, N.J.: Quantitative paleoenvironmental and paleoclimatic
699 reconstruction using paleosols, Earth Sci. Rev., 95, 1–52, 2009.

700 Sheldon, N.D., Retallack, G.J., and Tanaka, S.: Geochemical climofunctions from North
701 American soils and application to paleosols across the Eocene-Oligocene boundary in Oregon, J.
702 Geol., 110, 687–696, 2002.

703 Sloan, L.C.: Equable climates during the early Eocene: Significance of regional paleogeography
704 for North American climate, Geology, 22, 881–884, 1994.

705 Sloan, L.C., and Barron, E.: "Equable" climates during Earth history, Geology, 18, 489–492,
706 1990.

707 Smith, M.E., Carroll, A.R., and Singer, B.S.: Synoptic reconstruction of a major ancient lake
708 system: Eocene Green River, western United States, Geol. Soc. Am. Bull., 120, 54–84, 2008.

709 Smith, M.E., Chamberlain, K.R., Singer, B.S., and Carroll, A.R.: Eocene clocks agree: coeval
710 $^{40}Ar/^{39}Ar$, U-Pb, and astronomical ages from the Green River Formation, Geology, 38, 527–530,
711 2010.

712 Smith, M.E., Carroll, A.R., Scott, J.J., and Singer, B.S.: Early Eocene carbon isotope excursions
713 and landscape destabilization at eccentricity minima: Green River Formation of Wyoming, Earth
714 Planet. Sc. Lett., 403, 393–406, 2014.

715 Smith, M.E., Carroll, A.R., and Scott, J.J.: Stratigraphic expression of climate tectonism, and
716 geomorphic forcing in an underfilled lake basin: Wilkins Peak Member of the Green River
717 Formation, In Smith, M.E. and Carroll, A.R. (Eds.), Stratigraphy and Paleolimnology of the
718 Green River Formation, Springer (Dordrecht, NE), 61–102, 2015.

719 Smithsonian Institution Museum of Natural History Paleobiology (SIMNHP): Paleobiology
720 Database, Smithsonian Institution (Washington, DC), http://www.nmnh.si.edu/, 2015.

721 Snell, K.E., Thrasher, B.L., Eiler, J.M., Koch, P.L., Sloan, L.C., and Tabor, N.J.: Hot summers in
722 the Bighorn Basin during the early Paleogene, Geology, 41, 55–58, 2013.

723 Suarez, M.B., Passey, B.H., and Kaakinen, A.: Paleosol carbonate multiple isotopologue
724 signature of active East Asian summer monsoons during the late Miocene and Pliocene,
725 Geology, 39, 1151–1154, 2011.

726 Spicer, R.A., and Parrish, J.T.: Late Cretaceous–early Tertiary paleoclimates of northern high
727 latitude: a quantitative view, J. Geol. Soc., 147, 329–341, 1990.

728 Spicer, R.A., Herman, A.B., Liao, W., Spicer, T.E.V., Kodrul, T.M., Yang, J., and Jin, J.: Cool
729 tropics in the Middle Eocene: Evidence from the Changchang Flora, Hainan Island, China,
730 Palaeogeogr. Palaeocl., 412, 1–16, 2014.

731 Stinchcomb, G.E., Nordt, L.C., Driese, S.G., Lukens, W.E., Williamson, F.C., and Tubbs, J.D.:
732 A data-driven spline model designed to predict paleoclimate using paleosol geochemistry, Am. J.
733 Sci., 316, 746–777, 2016.

734 Takeuchi, A., Larson, P.B., and Suzuki, K.: Influence of paleorelief on the Mid-Miocene climate
735 variation in southeastern Washington, northeastern Oregon, and western Idaho, USA,
736 Palaeogeogr. Palaeocl., 254, 462-476, 2007.

737 Thompson, R.S., Anderson, K.H., Pelltier, R.T., Strickland, L.E., Bartlein, P.J., and Shafer, S.L.:
738 Quantitative estimation of climatic parameters from vegetation data in North America by the
739 mutual climatic range technique, Quat. Sci. Rev., 51, 18–39, 2012.

740 Thrasher, B.L., and Sloan, L.C.: Carbon dioxide and the early Eocene climate of western North
741 America, Geology, 37, 807–810, 2009.

742 Thrasher, B.L., and Sloan, L.C.: Land cover influences on the regional climate of western North
743 America during the early Eocene, Global Planet. Change, 72, 25–31, 2010.

744 TROPICOS: Global Plant Database: Missouri Botanical Garden (St. Louis, MO),
745 http://www.tropicos.org//, 2015.

746 United States Department of Agriculture (USDA): The PLANTS Database: NRCS National
747 Plant Data Team (Greensboro, NC), http://plants.usda.gov, 2015.

748 Utescher, T., Bruch, A., Erdei, B., Francois, L., Ivanov, D., Jacques, F., Kern, A., Liu, Y.,
749 Mossbrugger, V., and Spicer, R.: The Coexistence Approach- Theoretical background and
750 practical considerations of using plant fossils for climate quantification, Palaeogeogr. Palaeocl.,
751 10, 58–73, 2014.

752 Wang, Q., Ferguson, D.K., Feng, G., Ablaev, A.G., Wang, Y., Yang, J., Li, Y., and Li, C.:
753 Climatic change during the Palaeocene to Eocene based on fossil plants from Fushun China,
754 Palaeogeogr. Palaeocl., 295, 323–331, 2010.

755 West, C.K., Greenwood, D.R., and Basinger, J.F.: Was the Arctic Eocene 'rainforest' monsoonal?
756 Estimates of seasonal precipitation from early Eocene megafloras from Ellesmere Island,
757 Nunavut, Earth Planet. Sc. Lett., 427, 18–30, 2015.

758 Wilf, P.: Using fossil plants to understand global change: Evidence for Paleocene-Eocene
759 warming in the greater Green River Basin of southwestern Wyoming, University of
760 Pennsylvania (Philadelphia, PA), 384 pp., 1998.

761 Wilf, P.: Late Paleocene-early Eocene climate changes in southwestern Wyoming:
762 Paleobotanical analysis, Geol. Soc. Am. Bull., 112, 292–307, 2000.

763 Wing, S.L.: Late Paleocene-early Eocene floral and climatic change in the Bighorn Basin,
764 Wyoming, In Aubrey, M., Lucas, S., and Berggren, W. (Eds.), Columbia University Press (New
765 York, NY), 380–400, 1998.

766 Wolfe, J.A.: A paleobotanical interpretation of Tertiary climates in the Northern Hemisphere,
767 Am. J. Sci., 66, 691–703, 1978.

768 Wolfe, J.A.: Paleoclimatic estimates from Tertiary leaf assemblages: Ann. Rev. Earth Planet.
769 Sci., 23, 119–142, 1995.

770 Wolfe, J.A., and Wehr, W.: Middle Eocene dicotyledonous plants from Republic, northeastern
771 Washington, USGS Bull., 1597, 67 pp., 1987.

772 Wolfe, J.A., Forest, C.E., and Molnar, P.: Paleobotanical evidence of Eocene and Oligocene
773 paleoaltitudes in midlatitude western North America, Geol. Soc. Am. Bull., 110, 664–678, 1998.

774 World Climate Research Programme: Climate Model Intercomparison Project (Phase 5),
775 https://cmip.llnl.gov/, 2011.

776 Zaarur, S., Affek, H.P., and Brandon, M.: A revised calibration of the clumped isotope
777 thermometer, Earth Planet. Sc. Lett., 382, 47–57, 2013.

778 Zachos, J., Pagani, M., Sloan, L., Thomas, E., and Billups, K.: Trends, rhythms, and aberrations
779 in global climate 65 Ma to Present, Science, 292, 686–693, 2001.

780 Zachos, J.C., Dickens, G.R., and Zeebe, R.E.: An early Cenozoic perspective on greenhouse
781 warming and carbon-cycle dynamics, Nature, 451, 279–283, 2008.

782 Zamanian, K., Pustovoytov, K., and Kuzyakov, Y.: Pedogenic carbonates: Forms and formation
783 processes, Earth Sci. Rev., 157, 1–17, 2016.

784 **Figure Captions.**

785 **Figure 1.** Map and stratigraphy of the Green River Basin. A) Map of the region, showing major
786 sedimentary basins and topographic highs. Stars show proxy record sampling sites (paleosols in
787 yellow, paleoflora in red), and dashed box is the sampling region for modern climate stations and
788 the downscaling domain for both models. CF = Cordilleran fold-thrust belt, UU = Uinta uplift,
789 WR = Wind River uplift, OC = Owl Creek uplift, GM = Granite Mountains, FR = Front Range.
790 B) Simplified stratigraphy of the central to eastern GRB, showing facies for the Green River
791 Formation (GRF) and the equivalent and interfingering Wasatch Formation (WF) based on the
792 work of Smith et al. (2015) and Hyland and Sheldon (2013). LY = Lysitean, BF = Blacksforkian,
793 LU = Luman Member, NT = Niland Tongue, TM = Tipton Member, WPM = Wilkins Peak
794 Member, LA = Laney Member, RR = Ramsey Ranch Member, CB = Cathedral Bluffs Member.
795
796 **Figure 2.** Paleosol carbonate descriptions. A) Paired transmitted light and cathodoluminescence
797 (CL) images of carbonate nodules showing primary micrite in sampled nodules (I-II) and
798 diagenetically altered material in unsampled nodules (III-IV). Images taken on a Premier ELM-
799 3R Luminoscope at 8–10 kV, 0.5 mA, and 6.6–13.3 Pa with preset 1 s exposure; scale bars ~50
800 μm. B) Clumped isotope-based soil temperature profiles from discrete layers sampled within
801 analyzed paleosol exemplars. Profile HB-129 contained nodular carbonate layers at 20–30 cm,
802 50–65 cm, and 80–100 cm; Profile HB-187 contained nodular carbonate layers at 150–170 cm,
803 190–205 cm, and 240–260 cm.
804
805 **Figure 3.** Floral methods description. A) Probability density functions of hypothetical Taxa A
806 and B along climatic variable X to form a PDF representative of the maximum likelihood of co-

807 occurrence. B) Hypothetical climatic envelope of Taxon Q with climatic variables X and Y,
808 where point R occurs outside the envelope of Taxon Q but within its range of both variables
809 (creating a false inclusion of point R). C) Probability density function distributions for seasonal
810 temperatures from sampled paleofloral sites, where arrows indicate calculated mean
811 temperatures for each parameter, and n = number of morphotypes included in assemblage.
812
813 **Figure 4.** Temperature proxy estimates of CMMT (white), MAT (gray), and WMMT (black)
814 through the early Eocene. Triangles represent paleobotanical coexistence estimates, squares
815 represent paleosol geochemistry estimates, stars represent revised paleobotanical physiognomy
816 estimates, and circles represent clumped isotope estimates. Error bars represent PDF 2σ
817 (paleobotanical coexistence), root mean squared error ($PPM_{1.0}$ paleosol geochemistry),
818 calibration standard error (paleobotanical physiognomy), and propagated analytical/calibration
819 error (clumped isotopes). Shading highlights peak EECO conditions based on previous work
820 (e.g., Hyland et al., 2017), long dashed line highlights possible aliasing due to a long sampling
821 interval, and short dashed line highlights exclusion of two clumped isotope data points (see
822 Discussion). Estimates of peak EECO (51 ±0.5 Ma) and non-peak EECO MART are defined as
823 described in Table 1 and the Discussion, with MAT shown by vertical lines. Modern MART and
824 MAT are from averaged climate normals for NOAA weather stations in the GRB (NCDC, 2010).
825
826 **Figure 5.** Averaged monthly mean temperatures in the GRB, including: modern instrumental
827 data (filled black circles; NCDC, 2010); high (red squares; RCP8.5) and low (red circles;
828 RCP4.5) future emissions scenarios (PCDMI, 2014); high (blue squares; HiCO) and low (blue
829 circles; LoCO) early Eocene pCO_2 scenarios (Thrasher and Sloan, 2009; 2010); and proxy

reconstructions of WMMT and CMMT for non-peak (filled triangles) and peak EECO (open triangles) from this study. Method-averaged MART estimates shown for each category (symbols/colors match main panel).

Table 1. Comparison of Eocene MART estimates using different constraining temperatures and calculation methods.

Supplement.

A. Paleosol Data

Table A.1. Paleosol geochemistry data

B. Isotope Data

Table B.1. Clumped isotope data summary

Table B.2 Clumped isotope data full

C. Floral Data

Table C.1. Floral lists and NLR data

Table C.2. Climatic envelopes for plant taxa

Table C.3. Mean annual temperature estimates

D. Modeling Data

Table D.1. Modern climate data and model outputs

Table 1.

Interval	CMMT*	MAT*	WMMT*	MARTT†	MARTC†	MARTW†
peak EECO *(50.5 - 51.5 Ma)*	--	15.4˚C	28.2˚C	--	--	26˚C (4)
non-peak EECO *(53.5 - 51.5 Ma & 50.5 - 49.5 Ma)*	5.9˚C	15.6˚C	26.8˚C	22˚C (1)	21˚C (1)	23˚C (1)

MARTT = WMMT-CMMT
MARTC = (MAT-CMMT)×2
MARTW = (WMMT-MAT)×2
* Average of all available temperature proxy data across indicated time interval.
† Average MART estimate for each calculation method, number in parentheses is S.D. of calculation group.

Figure 1.

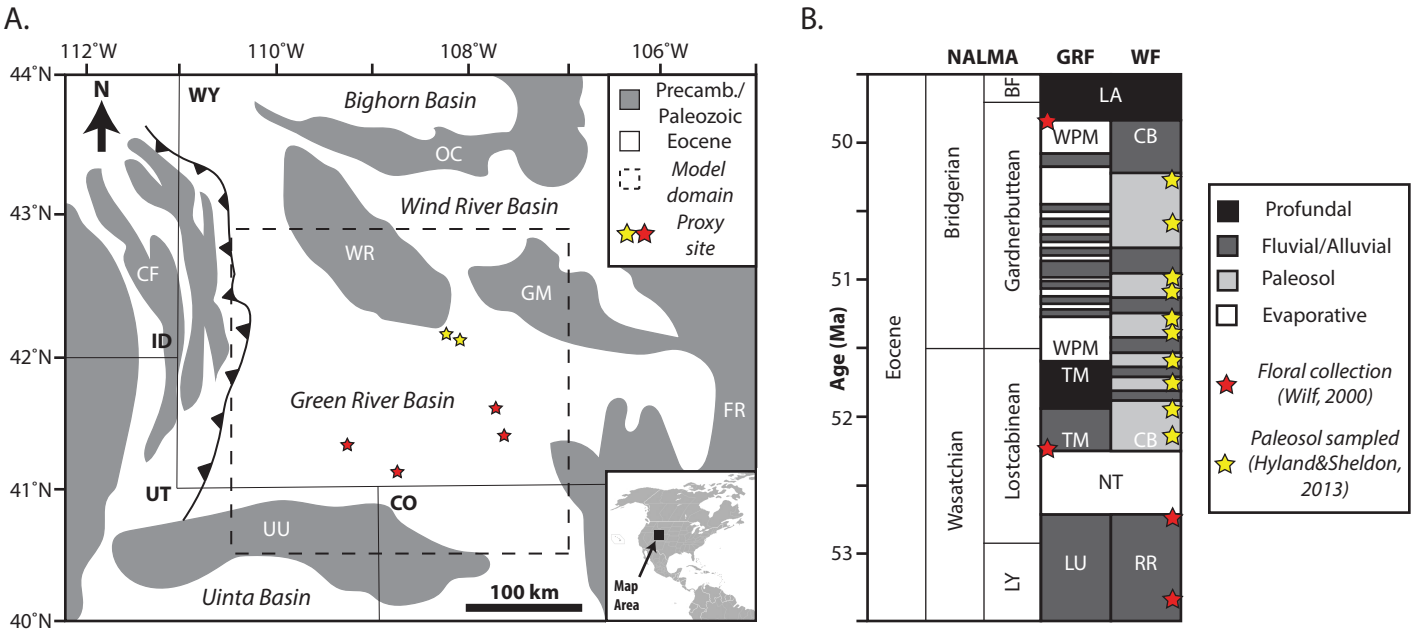
A.
112°W
110°W
108°W
106°W
44°N
43°N
42°N
41°N
40°N
N
WY
ID
UT
CO
CF
WR
GM
OC
FR
UU
Bighorn Basin
Wind River Basin
Green River Basin
Uinta Basin
100 km
Map Area
Precamb./ Paleozoic
Eocene
Model domain
Proxy site
B.
NALMA
GRF
WF
Age (Ma)
50
51
52
53
Eocene
Bridgerian
Wasatchian
BF
Gardnerbuttean
Lostcabinean
LY
LA
WPM
CB
TM
NT
LU
RR
Profundal
Fluvial/Alluvial
Paleosol
Evaporative
Floral collection (Wilf, 2000)
Paleosol sampled (Hyland&Sheldon, 2013)

Figure 2.

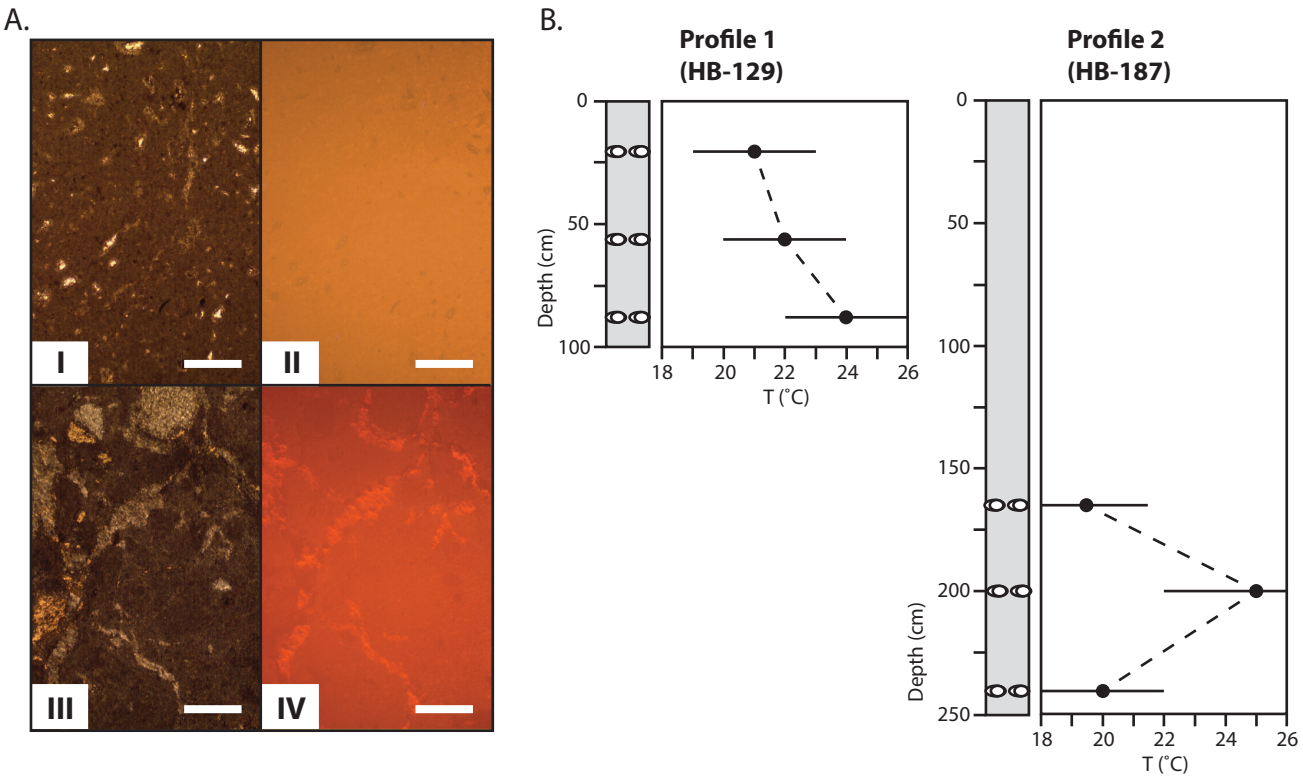
A.
I
II
III
IV
B.
Profile 1
(HB-129)
Profile 2
(HB-187)
Depth (cm)
T (°C)
0
50
100
150
200
250
18
20
22
24
26

Figure 3.

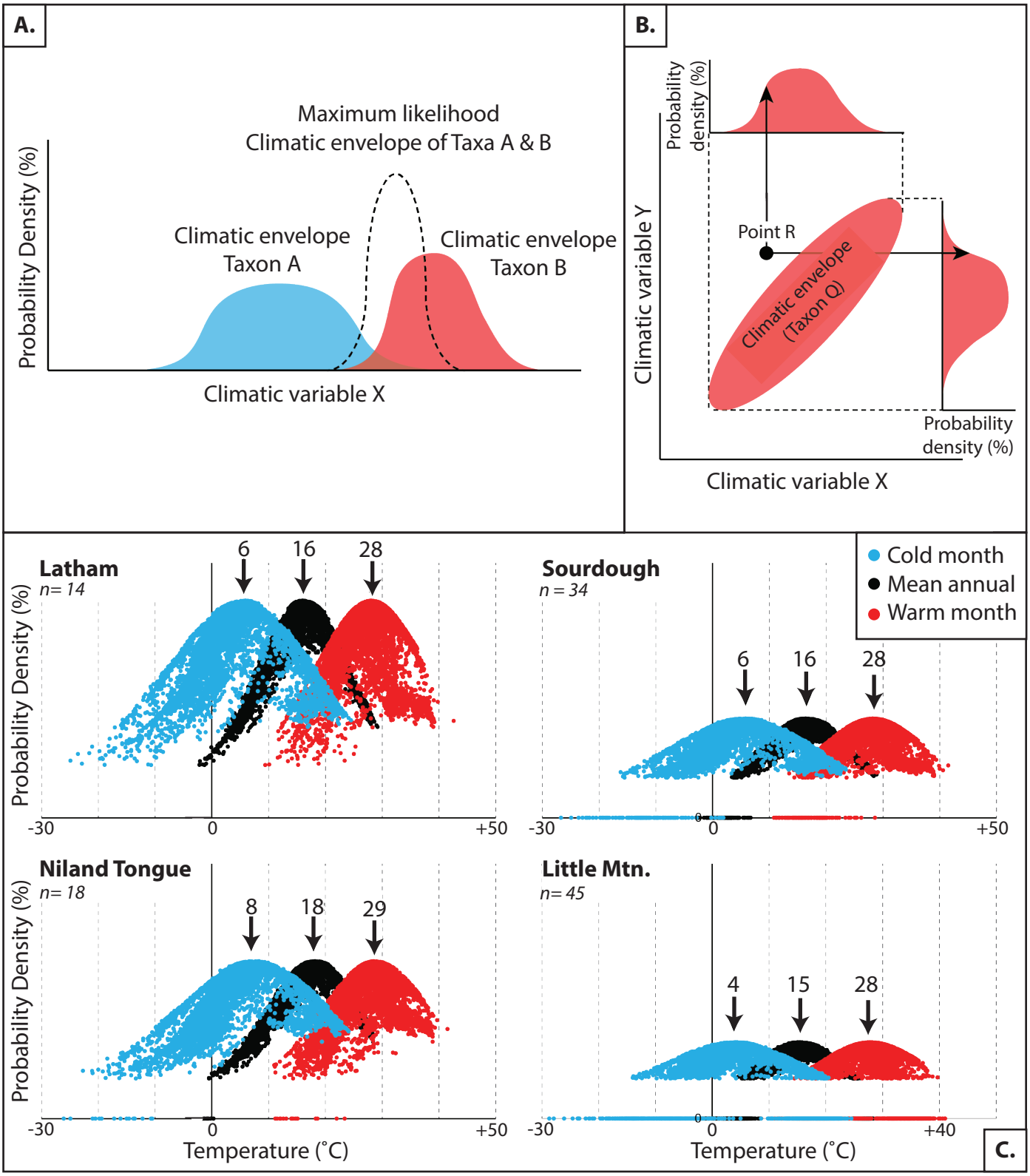
A.
Maximum likelihood
Climatic envelope of Taxa A & B
Probability Density (%)
Climatic envelope
Taxon A
Climatic envelope
Taxon B
Climatic variable X
B.
Probability
density (%)
Point R
Climatic envelope
(Taxon Q)
Climatic variable Y
Probability
density (%)
Climatic variable X
Cold month
Mean annual
Warm month
Latham
n= 14
6
16
28
Sourdough
n = 34
Niland Tongue
n= 18
8
18
29
Little Mtn.
n= 45
4
15
28
Probability Density (%)
-30
0
+50
+40
Temperature (˚C)
C.

Figure 4.

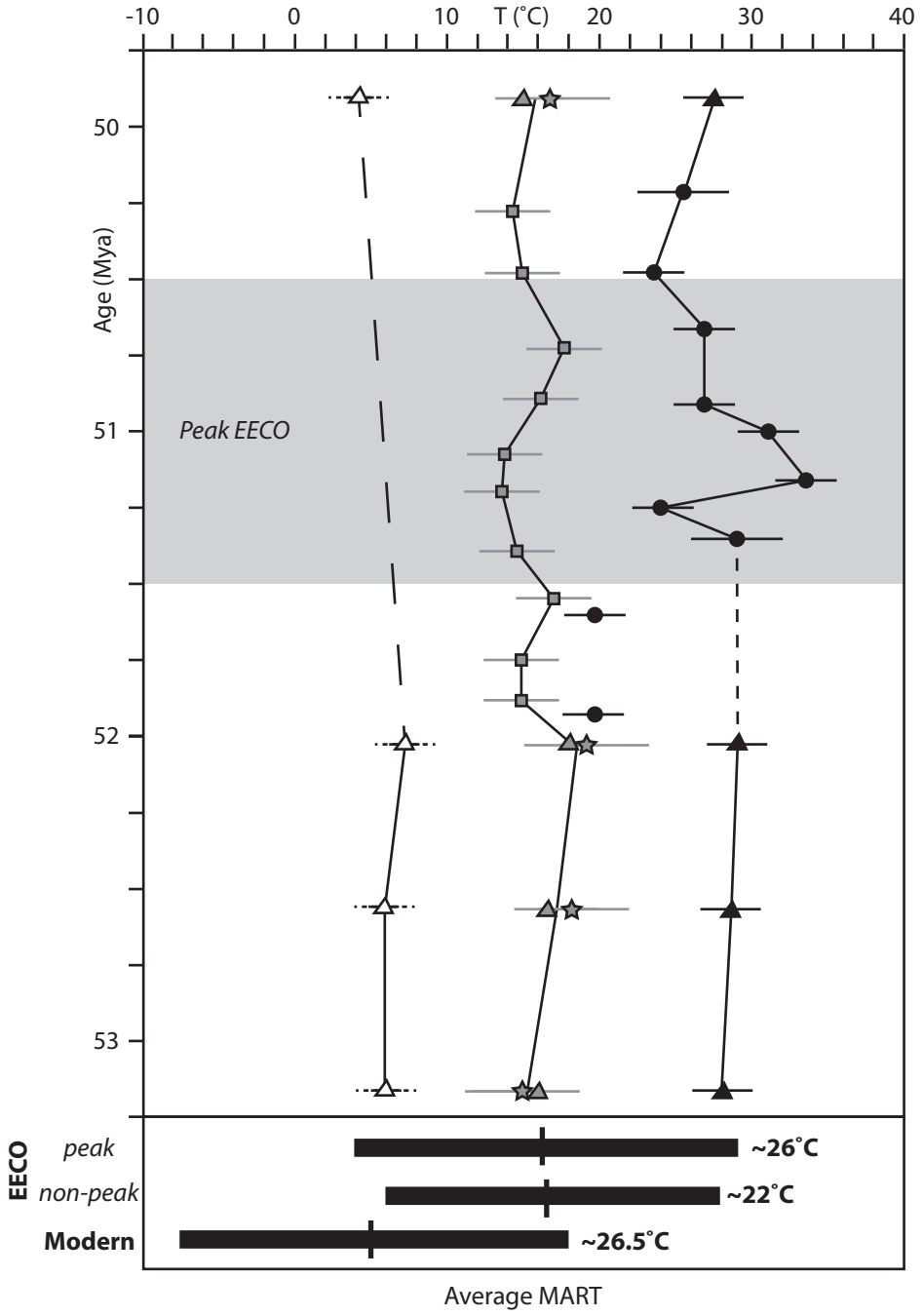
-10
0
10
T (˚C)
20
30
40
50
51
52
53
Age (Mya)
Peak EECO
EECO
peak
non-peak
Modern
~26˚C
~22˚C
~26.5˚C
Average MART

Figure 5.

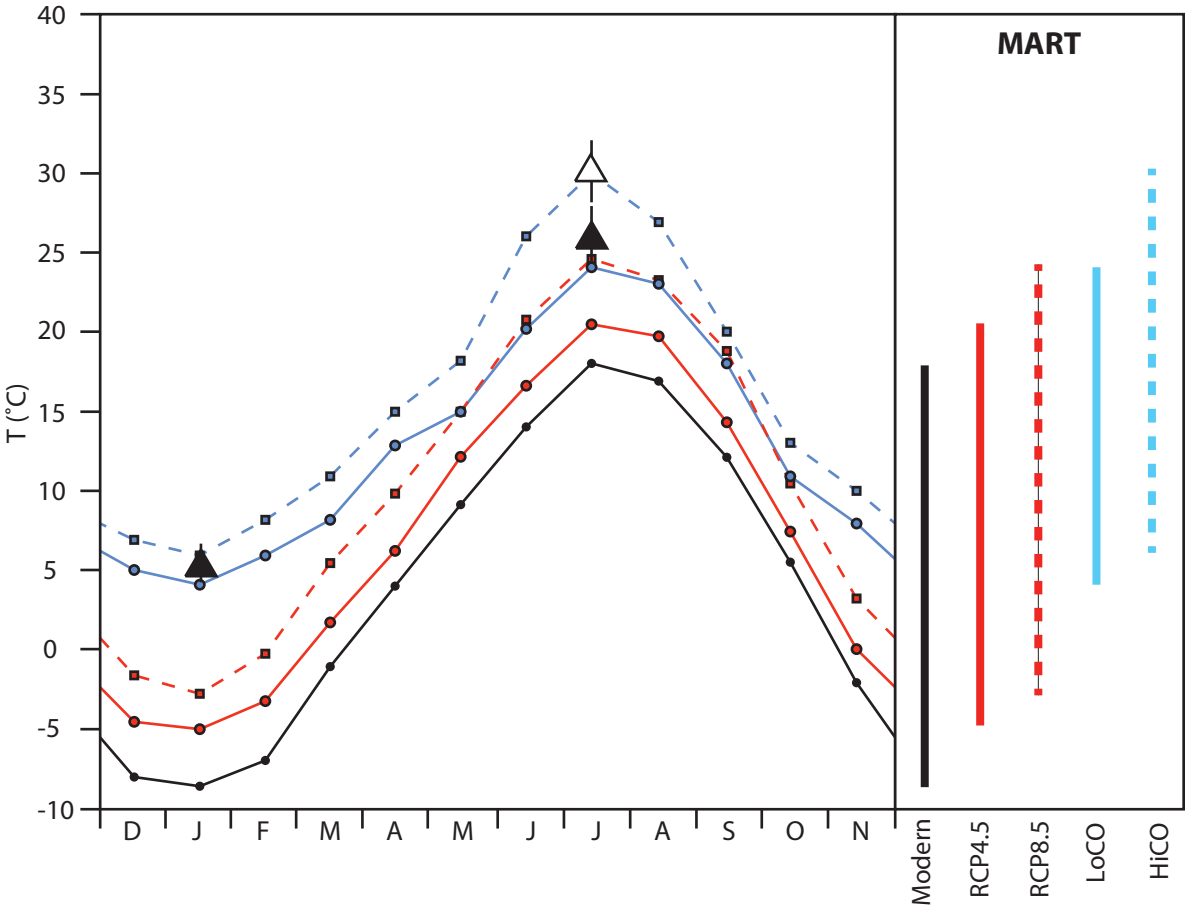
MART
T (°C)
40
35
30
25
20
15
10
5
0
-5
-10
D
J
F
M
A
M
J
J
A
S
O
N
Modern
RCP4.5
RCP8.5
LoCO
HiCO